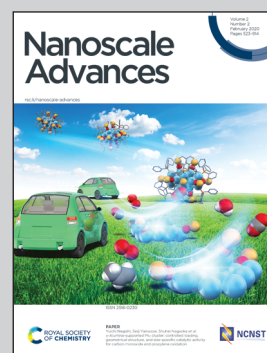


**Showcasing research from Professor Enoch Y. Park's laboratory, Research Institute of Green Science and Technology, Shizuoka University, Japan.**

The detection and identification of dengue virus serotypes with quantum dot and AuNP regulated localized surface plasmon resonance

The detection of dengue virus (DENV) serotypes has been described here, based on the distance dependent localized surface plasmon resonance (LSPR) between CdSeTeS QDs and AuNPs, which generates an altered fluorescence signal for each serotype of DENV. In the reaction mixture of hairpin nanoprobe and functionalized AuNPs, the addition of analyte oligos of DENV can open the hairpin structure of the nanoprobe to form various structures depending on the serotypes initiating the LSPR enhancement or the quenching effect on the QD fluorescence.

**As featured in:**




See Enoch Y. Park *et al.*,  
*Nanoscale Adv.*, 2020, **2**, 699.

## PAPER

[View Article Online](#)  
[View Journal](#) | [View Issue](#)Cite this: *Nanoscale Adv.*, 2020, 2, 699

# The detection and identification of dengue virus serotypes with quantum dot and AuNP regulated localized surface plasmon resonance†

Ankan Dutta Chowdhury,<sup>a</sup> Kenshin Takemura,<sup>b</sup> Indra Memdi Khorish,<sup>c</sup>  
Fahmida Nasrin,<sup>b</sup> Mya Myat Ngwe Tun,<sup>d</sup> Kouichi Morita<sup>d</sup> and Enoch Y. Park \*<sup>abc</sup>

The dengue hemorrhagic fever or dengue shock syndrome has become a severe human fatal disease caused by infection with one of the four closely related but serologically distinct dengue viruses (DENVs). All four dengue serotypes are currently co-circulating throughout the subtropics and tropics. Since the fatality rate increases severely when a secondary infection occurs by a virus serotype different from that of the initial infection, serotype identification is equally important as virus detection. In this study, the development and validation of a rapid and quantitative DENV serotype-specific (serotypes 1–4) biosensor are reported by optimizing the stable system between cadmium selenide tellurium sulphide fluorescent quantum dots (CdSeTeS QDs) and gold nanoparticles (AuNPs). Four different nanoprobe are designed using each primer–probe serotype-specific hairpin single-stranded DNA covalently bound at different positions to CdSeTeS QDs, which generates an altered fluorescence signal for each serotype of DENV. In fourplex reactions with free functionalized AuNPs and the four nanoprobe, the standard dilutions of the target virus DNA from  $10^{-15}$  to  $10^{-10}$  M were successfully detected. The limit of detection was found to be in the femtomolar range for all four serotypes, where the serotype detection ability was undoubtedly established. To confirm the applicability of this sensing performance in long chained complex RNAs, the sensor was also applied successfully to RNAs extracted from DENV culture fluids for serotype identification as well as quantification, which can lead to a potential diagnostic probe for point-of-care detection.

Received 4th October 2019  
Accepted 12th December 2019

DOI: 10.1039/c9na00763f

[rsc.li/nanoscale-advances](http://rsc.li/nanoscale-advances)

## Introduction

Metallic nanoparticles such as Au, Ag, and Pt influence the quantum yield of adjacent fluorophores in a manner dependent on the shape, size and concentration of the nanostructure.<sup>1–3</sup> Among the parameters, the absorption and emission of the fluorescent materials and the surface plasmon resonance wavelength of metal nanostructures, distance and spectral characteristics of nanoparticles play the most important roles in the fluorescence of the adjacent fluorophores.<sup>4–7</sup> If all these parameters are kept constant at their optimized conditions, fluorometric systems can be established by modulating the distance between metal nanoparticles and quantum dots (QDs)

based on their localized surface plasmon resonance (LSPR) effect. Recently, these types of systems have emerged as useful alternatives for enhancing the sensitivity of different detection platforms in biosensing.<sup>6,8–11</sup> The mechanism of plasmon enhancement or quenching can be mainly attributed to the change in the excitation rate due to a local field effect from the adjacent metal nanoparticles and the change in the emission rate by surface plasmon coupled emission, which can control the fluorescence intensity.<sup>2</sup> The application of plasmonic metallic nanoparticles in biosensing has been stimulated by the interaction of these nanoparticles with electromagnetic waves, which induces oscillations of the plasmons (free electrons) at the particle surface.<sup>1</sup> This phenomenon has led to the development of LSPR-based biosensors for various analytes. To optimize the distance between fluorescent QDs and metal nanoparticles, short chained oligomers can be used as potential linkers. Different surface plasmon resonance effects can be achieved on QDs by varying the length of the oligomers, which can be used as new biosensor systems for DNA/RNA detection.

The development of ultrasensitive DNA/RNA detection has been in great demand over the last decade for its various biomedical applications, including gene profiling, drug diffusion, and clinical diagnostics.<sup>12–17</sup> The development of DNA/RNA

<sup>a</sup>Research Institute of Green Science and Technology, Shizuoka University, 836 Ohya Suruga-ku, Shizuoka 422-8529, Japan. E-mail: [park.enoch@shizuoka.ac.jp](mailto:park.enoch@shizuoka.ac.jp)<sup>b</sup>Department of Bioscience, Graduate School of Science and Technology, Shizuoka University, 836 Ohya Suruga-ku, Shizuoka 422-8529, Japan<sup>c</sup>College of Agriculture, Graduate School of Integrated Science and Technology, Shizuoka University, 836 Ohya Suruga-ku, Shizuoka 422-8529, Japan<sup>d</sup>Department of Virology, Institute of Tropical Medicine, Nagasaki University, Sakamoto 1-12-4, Nagasaki City 852-8523, Japan

† Electronic supplementary information (ESI) available. See DOI: 10.1039/c9na00763f

detection methods in proper biosensing devices has great potential to gather maximum information from a small volume of analyte at a very low cost. In the case of viral disease detection, successful DNA/RNA based biosensors can offer significant advantages over existing diagnostic technologies such as PCR, antigen–antibody interaction or protein identification in terms of detection time and chances of reducing false positive responses.<sup>18,19</sup> Recently, a few fluorometric reports have claimed to achieve the desired low-level detection.<sup>20–22</sup> However, most of the detection protocols are highly dependent on PCR amplification. This still remains as the most challenging task to overcome this limitation. In case of dengue-like viral fever, which affects a significant and ever-increasing portion of the world's population annually, a low detection level without any further treatment is highly desired for the development of rapid detection tools. Recently, there have been many reports on dengue DNA detection by RT-PCR, electrochemical and fluorometric methods;<sup>23–28</sup> however, the successful application for point-of-care detection without any amplification step including the ability of serotype identification from clinically isolated RNA is rarely reported.

Herein, we report a new biosensing technique for the quantitative detection of DENV together with the determination of its serotype based on the distance-dependent LSPR between CdSeTeS QDs and AuNPs. Firstly, four different nanoprobees were designed as hairpin structures, where the loop portions of each hairpin are exactly complementary with the target analytes of four different DENV serotypes. The fixed regions of all the hairpins are self-complementary by six poly guanine (poly-G) and poly cytosine (poly-C), where one side is covalently bonded with CdSeTeS QDs. In addition, AuNPs functionalized with thiolated poly-C were also synthesized. In the sensing mixture of nanoprobees and the functionalized AuNPs, initially there should be no interaction between the AuNPs and the CdSeTeS QDs due to the closed hairpin

structure of the single-stranded probe DNA (ssDNA). However, after the addition of the complementary DNA/RNA of DENV, it can open the hairpin structure of the nanoprobe due to the better hybridization of the nanoprobe ssDNA and complementary RNA of DENV in its loop region, leaving the poly-G region of the nanoprobe free. The poly-C-functionalized AuNPs, which are free in the sensing solution, can undergo complementary binding with the free poly-G region of the nanoprobe (as depicted in Fig. 1). The hairpin region was designed as a highly conserved sequence on the serotype of analyte DENV RNA. The distance between the QDs and the AuNPs should be determined by the base pairs of the loop region at different positions, which triggers the LSPR enhancement (at around 14 nm) or quenching (at around 3 nm) effect on the fluorescence of the QDs, depending on the distance. It is noteworthy that the extent of the LSPR-fluorescence signal changes is completely dependent on the concentration of the target analytes in the optimized condition for sensing, creating a calibration curve in the concentration range of  $10^{-15}$  to  $10^{-10}$  M.

## Experimental

### Materials

Phosphate saline buffer (PBS, pH 7.4), methanol, potassium hydroxide, polyoxyethylene (20), sorbitan monolaurate (Tween 20), sulfuric acid, sodium citrate, tri-sodium citrate, hydrogen peroxide, chloroform and acetone were purchased from FUJIFILM Wako Pure Chemical Ind. Ltd. (Osaka, Japan). Tetramethylbenzidine (TMBZ) was purchased from Dojindo (Kumamoto, Japan).  $\text{HAuCl}_4$ , *N*-(3-dimethylaminopropyl)-*N*-ethylcarbodiimide hydrochloride (EDC), bovine serum albumin (BSA), *N*-hydroxysuccinimide (NHS), 1-octadecene, tellurium (Te), *L*-cysteine, hexadecylamine (HDA), cadmium oxide (CdO), trioctylphosphine oxide (TOPO), trioctylphosphine (TOP),

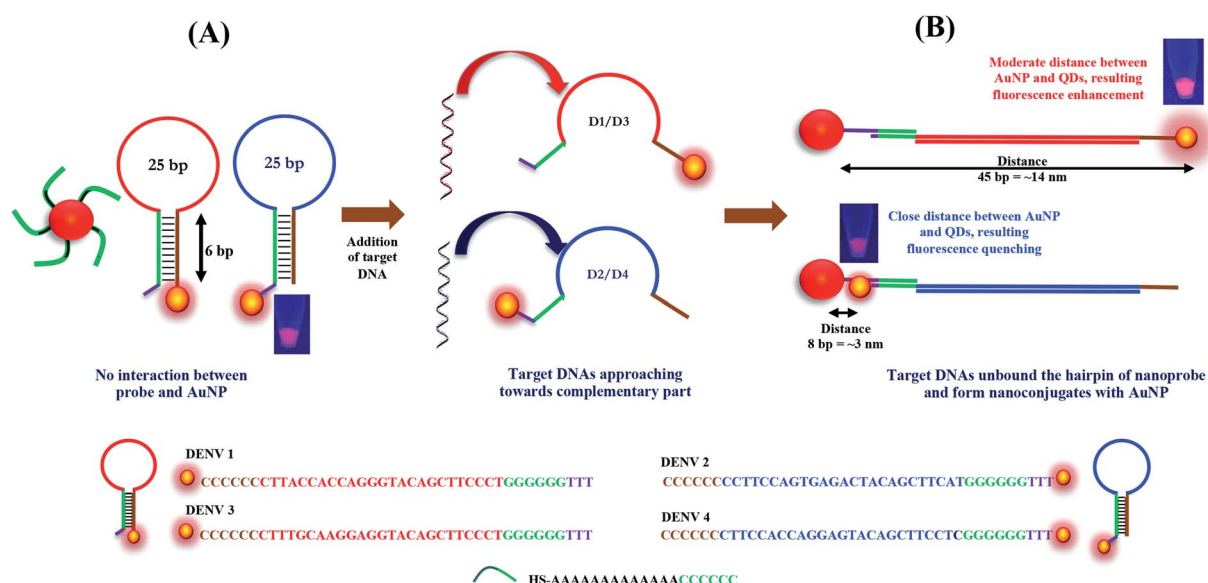


**Fig. 1** Schematic representation of the detection mechanism of DENV by AuNPs and hairpin ssDNA–CdSeTeS QDs. (A) Probe design for DProbe 1 and 2 and functionalized AuNPs. (B) Identification and fluorometric enhancement for DENV 1/3 serotype and quenching for DENV 2/4 serotype depending on the distance between the nanocomposite of AuNP–dsDNA–CdSeTeS.



selenium (Se) and sulfur (S) were purchased from Sigma Aldrich (Saint Louis, MO, USA). Oleic acid was purchased from Nacalai Tesque (Kyoto, Japan).

### Synthesis of CdSeTeS QDs

The synthesis of the CdSeTeS QDs was carried out according to the previously reported method *via* organometallic hot-injection synthesis with CdO, Se, Te and S as the basic precursors.<sup>29</sup>

### Synthesis of AuNPs

The synthesis of AuNP was carried out *via* the citrate reduction method. In brief, 35  $\mu$ L of 2 mM HAuCl<sub>4</sub> and 300  $\mu$ L of 100 mM tri-sodium citrate were added to 25 mL of pure boiling water in a 100 mL flask under vigorous stirring. Then the solution was boiled for 15 min until the color changed to pink. Subsequently, the AuNP solution was cooled to room temperature for further use.<sup>30</sup>

### Preparation of oligomeric solutions and DENV RNAs from DENV culture fluids

A calculated amount of diethyl pyrocarbonate (DEPC)-treated water, as estimated by the supplier, was added to a DNA-containing well, purchased from FASMAC (Atsugi, Japan) to obtain the concentration of 1 mM as the stock. The exact concentration of the DNA solutions was further verified by the absorption value at 260 nm in their UV-Visible spectrum (Table 1).

For the selectivity test, we purchased synthetic DNAs from FASMAC (Atsugi, Japan) of influenza virus (A/California/7/2009) (H1N1),<sup>31</sup> zika virus<sup>32</sup> and genogroup II RNA of norovirus<sup>33</sup> according to the used DNAs mentioned in the references of

their corresponding studies. In case of real sample analysis, DENV RNA was extracted from the DENV culture fluid using the High Pure RNA Isolation Kit (Roche Diagnostics, Mannheim, Germany) according to the manufacturer's instructions. The virus strains used for this study were clinical isolates from dengue patients in the Philippines as follows: DENV-1, strain 99St12A; DENV-2, strain 00St22A; DENV-3, strain SLMC50; and DENV-4, strain SLMC318.<sup>34</sup> These viruses were propagated onto C6/36 mosquito cell lines.

### Functionalization of AuNPs with SH-

AAAAAAAAAAACCCCCCT

The AuNP solution was stirred for 2 h with 0.1 mM of thiol-linked ssDNAs solution at pH 6.4, where the thiol group was covalently linked with the AuNPs. After successful functionalization of the AuNPs, the nanocomposite was washed several times with DI water and centrifuged at  $6000 \times g$  to obtain oligonucleotide-conjugated AuNPs free from excess probe ssDNA.

### Preparation of nanoprobe

The synthesized CdSeTeS QDs were incubated with different hairpin-structured probe ssDNAs of 0.1 mM, corresponding to each DENV serotype *via* the covalent interaction with the functionalized amine group of the probe ssDNAs and the -COOH group of CdSeTeS QDs to construct the nanoprobe.<sup>3</sup> In brief, 3 mg of EDC was first mixed with 10 mg of carboxylic-functionalized CdSeTeS QDs and then further activated with 5 mg of NHS for 30 min before the addition of functionalized ssDNAs. The reaction mixture was then stirred overnight for the maximum conjugation of the probe ssDNA with the QDs and then purified by centrifugation ( $3000 \times g$ ) for 5 min.

Table 1 The synthetic ssDNAs used in the present work

DNA	Sequences
Probe DNA 1	NH <sub>2</sub> -CCCCCCCCTTACCACCAGGGTACAGCTTCCCTGGGGGGTTT
Probe DNA 2	CCCCCCCCCTTCCAGTGAGACTACAGCTTCATGGGGGGTTT-NH <sub>2</sub>
Probe DNA 3	NH <sub>2</sub> -CCCCCCCCTTTGCAAGGAGGTACAGCTTCCCTGGGGGGTTT
Probe DNA 4	CCCCCCCCTTCCACCAGGAGTACAGCTTCTCCTGGGGGGTTT-NH <sub>2</sub>
Probe DNA for AuNP	SH-AAAAAAAAAAACCCCCCT
<b>Target DNAs</b>	
ssDNA 1 <sup>a</sup>	AGGGAAGCTGTACCCTGGTGGTAAG
ssDNA 2 <sup>a</sup>	ATGAAGCTGTAGTCTCACTGGAAG
ssDNA 3 <sup>a</sup>	AGGGAAGCTGTACCTCCTTGCAAG
ssDNA 4 <sup>a</sup>	GAGGAAGCTGTACTCCTGGTGAAG
<b>Target DNAs for selectivity</b>	
Influenza virus <sup>b</sup>	AAATACAACGGCATAATAACTGAAA <sup>31</sup>
Zika virus <sup>b</sup>	TGCTAAACGCGAGTAGCCCGTGT <sup>32</sup>
Norovirus <sup>b</sup>	TCCTGACATCATACAAGCTAACTCC <sup>33</sup>
<b>Real samples</b>	
Dengue RNAs	Given in Table S1 ESI, the region is marked in green color

<sup>a</sup> These synthetic ssDNAs were synthesized according to the conserved region of dengue RNAs, as presented in the ESI, marked in green colour.

<sup>b</sup> For the selectivity test, these synthetic ssDNAs were chosen from their corresponding references.



Consequently, four types of hairpin-structured DENV 1–4 nanoprobe were obtained.

### Physicochemical analysis

Transmission electron microscopy (TEM) images were obtained using a TEM (JEM-2100F; JEOL, Tokyo, Japan) operated at 200 kV to check the size and surface morphology of the as synthesized nanocomposites. UV-Vis absorption and fluorescence spectra were obtained using a filter-based multimode microplate reader (Infinite® F500; TECAN, Ltd, Männedorf, Switzerland). X-ray diffraction (XRD) was carried out for all samples in dried powder form using a RINT ULTIMA XRD (Rigaku Co., Tokyo, Japan) with an Ni filter and a Cu-K $\alpha$  source. Dynamic light scattering (DLS) measurements were performed using a Zetasizer Nano series (Malvern Inst. Ltd., Malvern, UK). The different chemical environments of the CdSeTeS QDs nanocomposites before and after the conjugation of AuNPs were accounted thorough FTIR (ATR 8700, Shimadzu Co., Tokyo, Japan). The samples were dried in an oven and then mixed homogeneously with dried crystals of KBr to make pellets. Then the pellets were immediately used for the FTIR analysis to avoid any water absorption.

### LSPR-mediated DENV serotype identification principle

Fig. 1 displays a schematic overview of the preparation and detection principle of the biosensor. Firstly, CdSeTeS QDs conjugated with the hairpin ssDNAs were synthesized, as mentioned above, and then mixed with the functionalized AuNP solution. There was no specific interaction occurring due to the close-loop structure of the hairpin ssDNA in the nanoprobe. However, after the addition of the target ssDNA/RNA sequences of each DENV serotype, the target ssDNAs opened up the complementary ssDNA loop sequence of the hairpin, forming a DNA/DNA or DNA/RNA hybridization. Thus, in this stage, a linear strand of the probe ssDNA conjugated with the QDs could be achieved, where the target DNA/RNAs were aligned with the nanoprobe through strong complementary binding. Initially, the synthetic ssDNA and probe ssDNAs were used for analysis. In the next case, real RNA samples were used for sensing. Before the addition of the target RNAs, they were heated to 95 °C to denature any secondary structure between themselves and then added to the sensing solution immediately at room temperature. The probe ssDNAs concentration was always maintained at  $1.1 \times 10^{-9}$  M while the target ssDNAs concentration was varied from  $10^{-9}$  to  $10^{-15}$  M. Since a slight excess amount of probe ssDNAs should not affect the fluorescence of the resulting solution (Fig. S1, ESI†), we used a slightly higher amount of probe ssDNAs with respect to the target ssDNA of 100  $\mu$ L. In addition, the poly-C-functionalized AuNPs, which were free in the sensing solution, also underwent complementary binding with the free poly-G region of the nanoprobe. Therefore, in all four cases of the DENV serotypes, the target DNA/RNAs formed a linear structure of AuNP-complementary DNA/RNA-CdSeTeS QDs. Depending on the nanoprobe design, the QDs should be present either in the far end or very close to the AuNP, as shown in the Fig. 1. Since the

enhancement or quenching of the fluorescence signal was triggered based on the distance between the QDs and the bonded plasmonic AuNPs, different changes in the signal occur with different analytes. The extent of the fluorescence enhancement/quenching of the QDs was dependent on the LSPR signal from the AuNPs, which was equivalent to the concentration of the target DNA/RNA.

## Results and discussion

### Characterization of CdSeTeS QD-dsDNA-AuNP nanocomposites

The TEM image of the as-synthesized AuNPs is shown in Fig. 2(A), where the spherical particle shape is consistently observed with a homogeneous distribution. The particle size distribution was calculated in Fig. 2(B) to be in the range of 30–50 nm with the average particle size of  $39 \pm 0.5$  nm. Since the particle size of the SPR molecule can influence the LSPR intensity significantly, the homogeneity of the AuNPs is highly desirable. Similarly, the as-synthesized CdSeTeS QDs were also analyzed *via* TEM, which had a particle size distributed in the range of 7–15 nm with the average particle size of  $11.4 \pm 0.5$  nm (Fig. 2(C)). The UV-Vis spectrum of the CdSeTeS QDs is presented in Fig. S2 of ESI†, showing the signature absorption hump of at 540 nm, which indicates their successful synthesis.<sup>29,35</sup> After the successful conjugation of the nanocomposites through the analyte ssDNA, CdSeTeS QD-dsDNA-AuNP was further characterized *via* TEM. For the characterization, the DENV 1 target analyte was used to construct the CdSeTeS QD-dsDNA-AuNP nanocomposite. Since the other 3 target ssDNAs have a similar structure with DENV 1 and form the identical nanocomposite conformation, all the characterizations were carried out for the CdSeTeS QD-dsDNA-AuNP nanocomposite with DENV 1. In Fig. 2(E), it is clearly observed from the image that the small sized QDs ( $\sim 5.9$  nm) (Fig. 2(D)) and the AuNPs ( $\sim 40$  nm) were closely arranged due to the covalent attachment controlled by the short linker of the ssDNA chain. The concentration of the AuNPs was much less than that of the CdSeTeS QDs concentration, and hence relatively high amounts of QD were found near each single AuNP (Fig. 2(E)). The nanocomposite formation was further verified by hydrodynamic diameter measurement, where the hydrodynamic diameter of the CdSeTeS QD-dsDNA-AuNP nanocomposite together with its individual components was determined by DLS (Fig. 2(F)). The bare CdSeTeS QDs and AuNPs showed a hydrodynamic size of  $7.5 \pm 0.5$  nm and  $27.4 \pm 1.5$  nm, respectively, which is slightly different than their solid-state size calculated from the TEM image. As small sized and charged particles, the QDs and the AuNP are well solvated in aqueous buffer medium, resulting in a decrease in their hydrodynamic radius.<sup>36</sup> In the case of the CdSeTeS QD-dsDNA-AuNP nanocomposite, it possessed a diameter of  $76 \pm 2.8$  nm, which is larger than its individual size, confirming its agglomerated distribution, which was also corroborated by the TEM image. In the case of the elemental mapping of an isolated cluster of the CdSeTeS QD-dsDNA-AuNPs nanocomposite, as depicted in Fig. 2(G), the individual elements can be observed distinctly. The



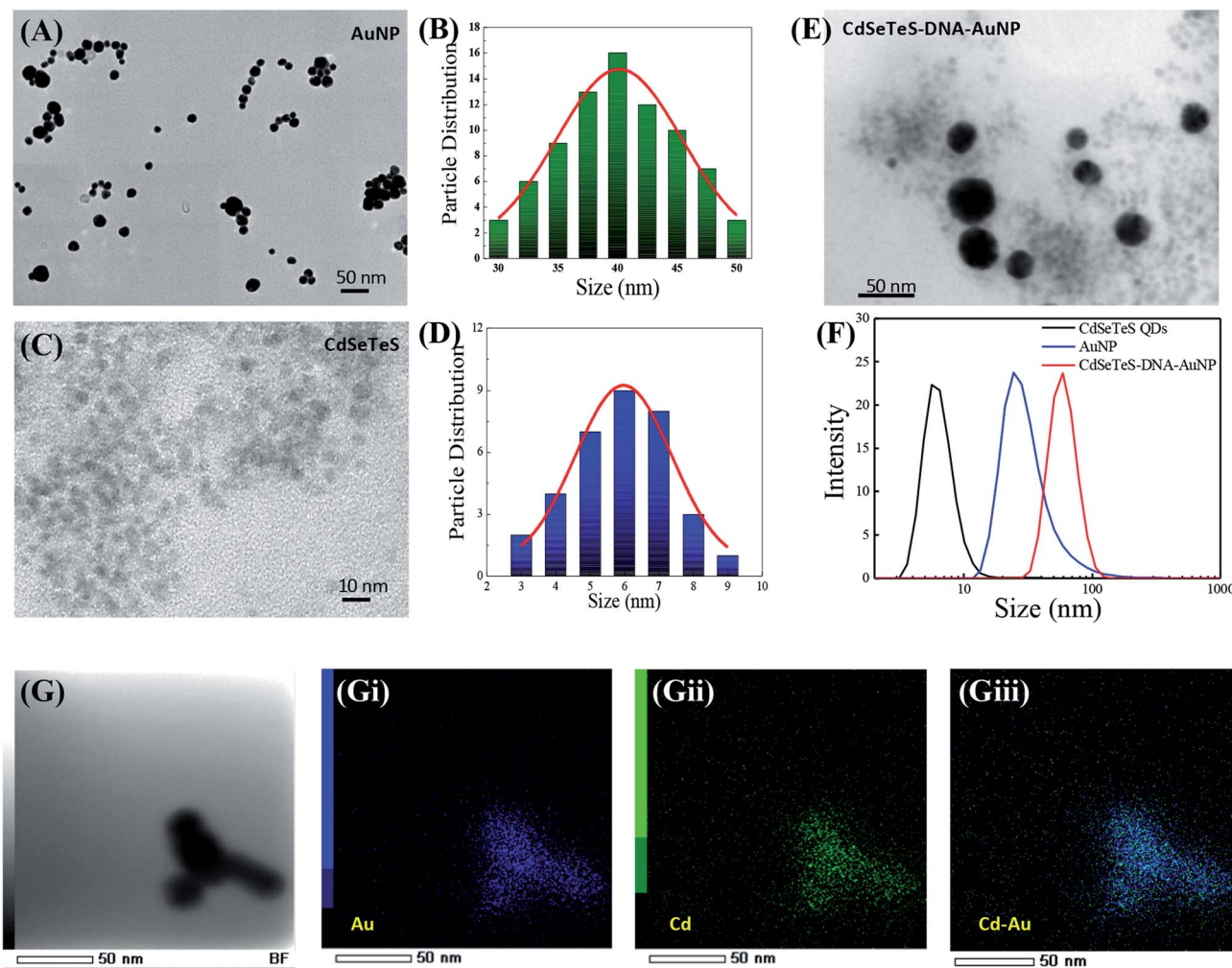


Fig. 2 TEM images and size distribution of AuNPs (A and B) and CdSeTeS QDs (C and D), respectively. (E) TEM image of CdSeTeS QDs–dsDNA–AuNPs, (F) DLS hydrodynamic sizes of CdSeTeS QDs, AuNP and CdSeTeS QDs–dsDNA–AuNP nanocomposites, and (G) STEM mapping of CdSeTeS QDs–dsDNA–AuNP, (Gi) Au, (Gii) Cd and (Giii) merged image.

nanocomposite was mapped with Au and Cd, as shown in Fig. 2(Gi) and 2(Gii), respectively, whereas their merged image in Fig. 2(Giii) proves the successful linkage of these two components of CdSeTeS QDs and AuNP by the ssDNA chain.

The nanocomposite was further characterized by XRD to illustrate the structural changes in its two crystalline components of CdSeTeS QDs and AuNPs. The crystalline nature of the bare AuNPs was confirmed by XRD analysis. In Fig. 3(A), the diffraction features of the bare AuNP show two characteristic peaks at  $38.1^\circ$  and  $44.6^\circ$ , corresponding to the (111) and (200) planes, respectively.<sup>37</sup> Similarly, the diffraction pattern of the bare CdSeTeS QDs indicates that the QDs are highly crystalline and cubic in nature (Fig. 3(A)), exhibiting three characteristic peaks at the 2 theta values of  $26.7^\circ$ ,  $44.2^\circ$  and  $51.8^\circ$  for the (111), (220) and (311) crystal planes, respectively.<sup>33</sup> It is noteworthy that the position of these peaks remained almost unchanged even after conjugation with the AuNPs, indicating that the attachment only takes place in the functional groups of the CdSeTeS QDs without affecting its own crystal lattice. In

addition, two small but clear peaks at  $2\theta = 38.1^\circ$  and  $44.6^\circ$  appeared in the spectrum due to the incorporation of the AuNPs on the nanocomposite, confirming the successful formation of the CdSeTeS QD–dsDNA–AuNPs. However, the relative intensities of the Au peaks decreased obviously and the Au peak at  $44.6^\circ$  partially overlapped with the peak at  $44.2^\circ$  for the CdSeTeS QDs since the contribution of AuNPs is much lower than that of the CdSeTeS QDs in the CdSeTeS QD–dsDNA–AuNPs nanocomposite. Therefore, it can be concluded from the XRD results that the structural conformation of the AuNPs and QDs remained the same even after the formation of the nanocomposite. Therefore, all the changes in the fluorescence originating from the nanocomposites solely depend on the LSPR effect.

FTIR spectroscopy analysis was also performed to reveal the conjugation of DNA with the AuNPs and its subsequent binding to the CdSeTeS QDs, as shown in Fig. 3(B). In the case of the bare CdSeTeS QDs, the spectrum exhibited all of their standard transmitted peaks as reported earlier, particularly at  $1735\text{ cm}^{-1}$ ,



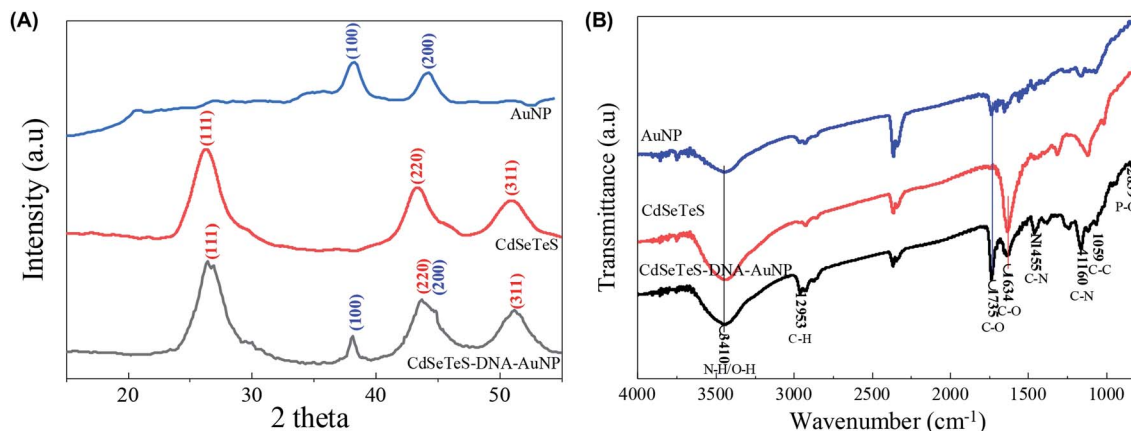


Fig. 3 Characterization of AuNP, CdSeTeS QDs and CdSeTeS-dsDNA-AuNP nanocomposites. XRD patterns (A) and FTIR spectra (B).

which is attributed to the asymmetric carboxylate ( $-\text{COO}^-$ ) group.<sup>33</sup> In case of the bare AuNPs, their FTIR spectrum revealed the presence of different functional groups such as hydroxyl, amine and  $-\text{COOH}$  linkages. In the case of the CdSeTeS QD-dsDNA-AuNPs nanocomposite, the bands observed at  $3410.1\text{ cm}^{-1}$ ,  $2953.3\text{ cm}^{-1}$  and  $1735.6\text{ cm}^{-1}$  correspond to the  $-\text{OH}/\text{NH}_2$  stretching, C-H stretching, and C-O stretching of carboxylic acid, respectively.<sup>38</sup> The band at  $1160\text{ cm}^{-1}$  represents the C-N stretching, which is quite common for DNA, indicating the presence of DNA in the AuNPs.<sup>39</sup> The band at  $1059\text{ cm}^{-1}$  is the characteristic peak assigned to the vibration of ribose (C-C sugar) or associated with the phosphate groups of DNA.<sup>40</sup> Another indicative peak was also observed at  $839\text{ cm}^{-1}$  for the antisymmetric vibration of the P-O bond of the phosphate group ( $839\text{ cm}^{-1}$ ) of DNA.<sup>41</sup> The combination of these characteristic peaks of the nanocomposite with DNA indicates the successful formation of AuNP-DNA with the CdSeTeS QDs.

### Designing four DENV nanoprobe for serotype detection employing the distance-dependent LSPR mechanism

LSPR originating from the surface resonance electrons of noble metal nanoparticles such as Au and Ag can have either enhancement or quenching effects on the adjacent fluorophore. This depends on the distance of the fluorophores separated from the metal nanoparticle and the relative position of the LSPR wavelength from the excitation or emission wavelength of the fluorophores.<sup>5</sup> The fluorescence property of the CdSeTeS QDs was measured by calculating their quantum efficiency (quantum yield = 0.33, given in Fig. S3, ESI†), which is quite satisfactory for this fluorometric investigation. Therefore, the quantum efficiency and the emission intensity of the CdSeTeS QD fluorophore can be enhanced or quenched by the surrounding metal AuNP *via* the equilibrium of the two-way electron transfer process of non-radiative energy transfer and local field enhancement effect.<sup>2</sup> When this duo is in very close proximity (for example  $\sim 2\text{ nm}$ ), non-radiative energy transfer dominates, which results in the quenching of the fluorescence. Due to the increased distance, the local field enhancement effect becomes significant, contributing to the enhancement in fluorescence intensity. The emission

intensity reaches maximum at an optimal distance of about 14–20 nm depending on the size and shape of both nanocomponents, as depicted in the schematic diagram in Fig. 4(A). When the distance is increased to more than 20 nm, the fluorescence intensity does not have any significant effect on the neighboring group of metal nanoparticles. Therefore, in case of a large distance from the AuNPs, the electric field intensity becomes insignificant, causing no observable changes in the emission intensity of the CdSeTeS QDs.

Thus, employing the distance-dependent fluorescence behavior, we designed four types of nanoprobe for four specific DENV serotypes. As illustrated in Fig. 4(B), four hairpin structures with 40 bp ssDNA oligonucleotides were synthesized, which consisted of a 5'/3' terminus with an amino group ( $\text{NH}_2$ ) for the conjugation of the CdSeTeS QDs. The probes contained 25 bp complementary sequences with four DENV serotypes assigned in four different colors in the scheme in Fig. 4(B). The remaining 15 bp were designed with 6 poly-G and 6 poly-C for the loop formation in addition with 3 bp T in the poly-C end. Therefore, after conjugation with the complementary DENV serotype ssDNA, the loop can be opened and the GGGGGGTTT region can be bonded with the free AuNP-SH-CCCCCCCCAAAAA probe, which is free in the sensing solution. The probe ssDNA has 6 G-C complementary binding, whereas 25 unbound nucleotides in the loop region. After the addition of the target ssDNAs, the conjugated structure contained 25 complementary bonded nucleotides with the target ssDNA and 6 new G-C binding with free AuNPs with 6 free nucleotides in the end, which indicates the higher stability of the conjugated structure over the former. Additionally, compared with similar studies on DNA hairpin, it can be concluded that the straight chain form of DNA has much higher stability than the looped form due to the much higher number of complementary DNA nucleotides.<sup>42–44</sup> Since the  $\text{NH}_2$  group is bonded with the ssDNA nanoprobe in the 5' end in the case of DENVs 2 and 4, the CdSeTeS QDs should be positioned very close to the AuNPs ( $< 6\text{ nm}$ ), resulting in quenching. On the other hand, in the case of DENVs 1 and 3, since the  $\text{NH}_2$  group is bonded with the ssDNA nanoprobe in



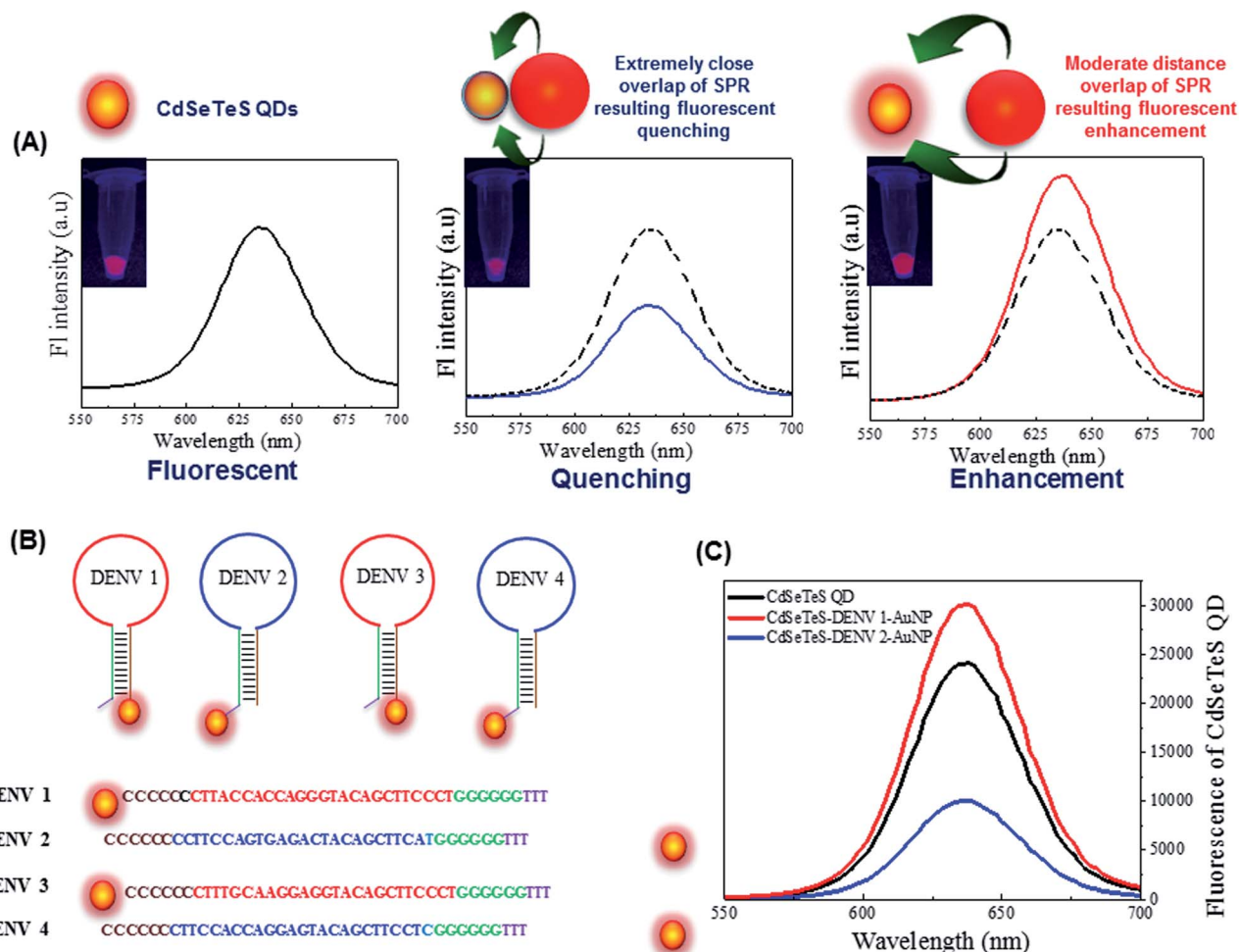


Fig. 4 (A) Schematic representation of the distance-based LSPR effect of AuNPs on CdSeTeS QDs, (B) schematic representation of the preparation of 4 types of hairpin probes for sensing, and (C) fluorescence properties of CdSeTeS QDs, and CdSeTeS QDs-dsDNA-AuNP nanocomposites with DENV 1 and DENV 2.

the 3' end, the distance between the AuNPs and the CdSeTeS QDs should be approx. 40 bp or 12–14 nm, resulting in a fluorescence enhancement. The initial fluorescence of the probe showed only the fluorescence of the QDs, as designated in the scheme in Fig. 1(A). However, the QD fluorescence increased in the presence of the AuNPs at a certain distance due to the LSPR effect. Therefore, after the addition of DENV 1/3, the target ssDNA bound the loop structure of the probe ssDNA and opened it in such way that the distance between the QDs and the AuNPs was  $\sim 14$  nm, which is perfect for the LSPR effect, resulting in an enhancement of the QD fluorescence from its initial value, as depicted in Fig. 1(B). These two types of conjugation are shown in Fig. 4(C), where DENV 1 enhances the fluorescence of CdSeTeS QDs, whereas the DENV 2 produces the quenching effect compared to the bare CdSeTeS QDs, supporting our hypothesis of this present work.

### DENV serotype detection

The nanoprobe of four types of ssDNA-CdSeTeS QDs and ssDNA-AuNPs were mixed with the 4 serotypes of DENV ssDNAs

(DENV-1, 2, 3 and 4), separately, for serotyping. From the different vials, we can obtain four different positioned CdSeTeS QD-DNA-AuNP nanocomposites, where the distance between the AuNPs and the CdSeTeS QDs was also different. The fluorescence intensity was recorded in the wavelength range of 500–700 nm upon the excitation of the CdSeTeS QDs at 480 nm. It is clear from the Fig. 5(A–D), the nanocomposites showed a fluorescence enhancement for DENVs 1 and 3 (Fig. 5(A) and (C)) and quenching for DENVs 2 and 4 (Fig. 5(B) and (D)), respectively. To check their cross reactivity, the interaction between all sixteen possible combination of the four nanoprobe with four serotype target DENV ssDNAs is presented in Fig. 5(E) and their schematic representation is shown in Fig. 5(F). It can be clearly observed that the assigned nanoprobe, which were designed for a specific DENV analyte, are very sensitive for the exact complementary target ssDNAs, where the other ssDNAs and the bare buffer medium show almost insignificant signals. In case of DProbe 1, the target DENV 1 showed a change in fluorescence of 17.1% with respect to the initial fluorescence, whereas the DENV 2, 3 and 4 showed



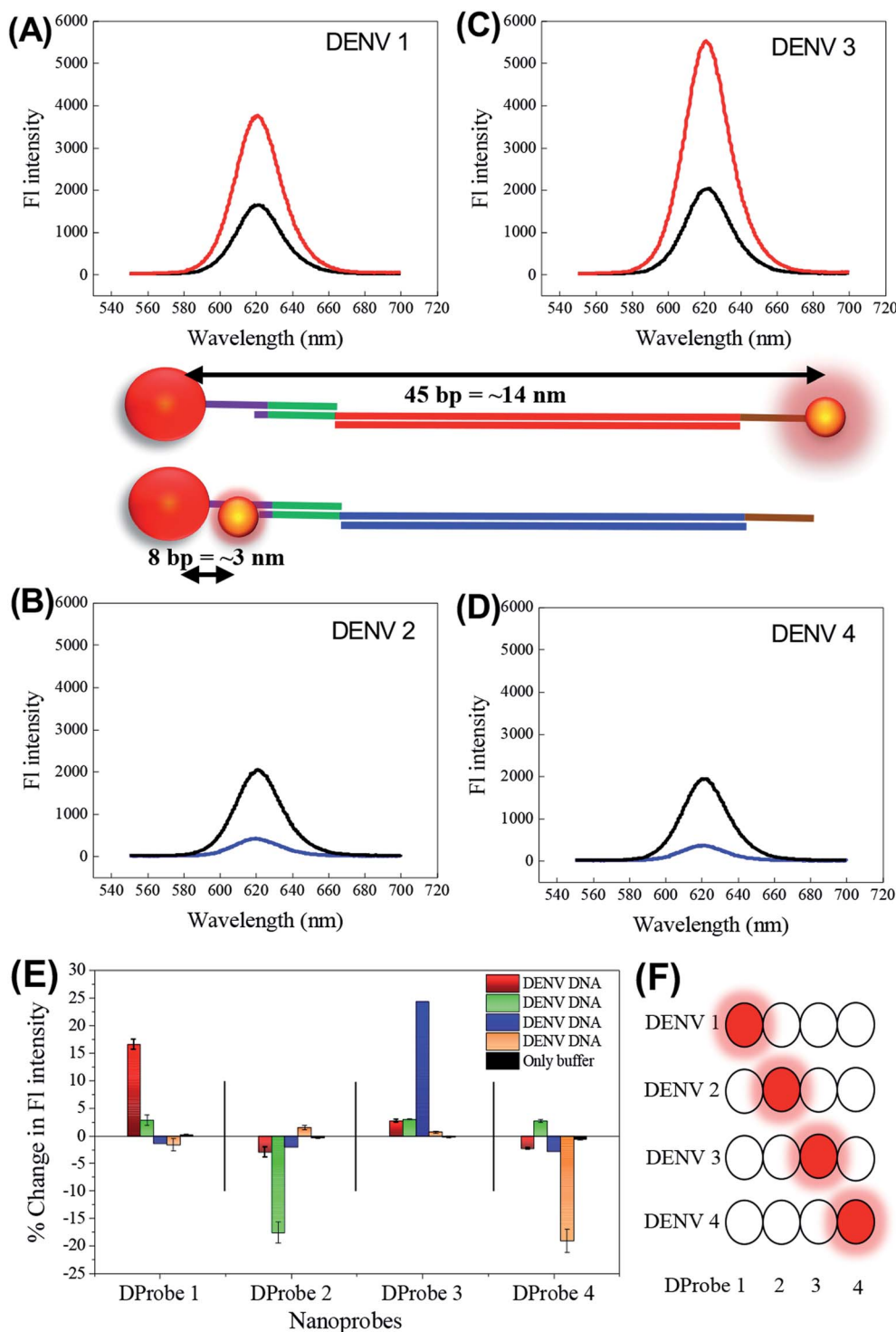


**Fig. 5** Distance-dependent fluorescence intensity changes of CdSeTeS QDs of the four different sensing nanoprobe in the presence of four different analytes of DENV 1 (A), DENV 2 (B), DENV 3 (C) and DENV 4 (D) serotypes. (E) Comparative bar diagram for the cross sensitivity of all four nanoprobe in the presence of all four types of DENV serotypes. (F) Pictorial illustration of the cross-reactivity determination of the sensor.

only the 2.3%, −1.4% and −1.6% changes, which are almost negligible compared with the target signals. Similar or better specificity was observed in case of DProbe 2, DProbe 3 and DProbe 4. Therefore, from the above results, we can obtain exact information about the DENV serotype. By changing the QDs

with different emission wavelengths in future, we can also distinguish the exact serotype in a one-pot reaction mixture.

#### Calibration for four DENV serotypes

After the successful identification of the serotype, the quantification of the target ssDNA was examined and expressed in



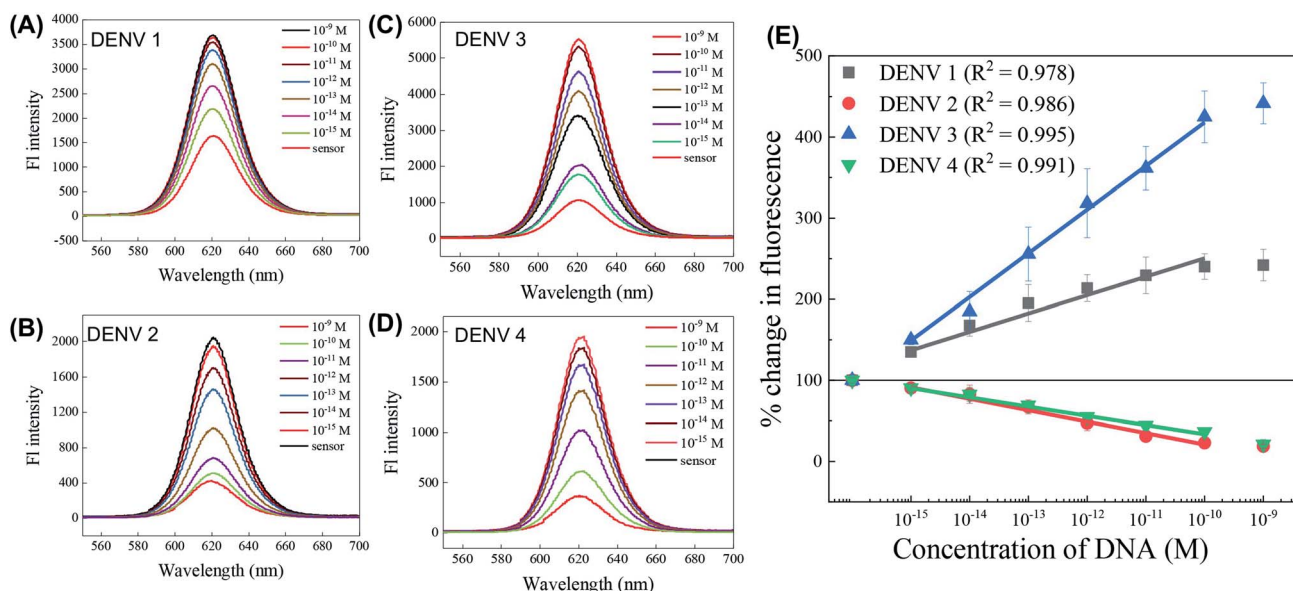


Fig. 6 (A–D) Concentration-dependent fluorescence changes of the CdSeTeS–dsDNA–AuNP nanocomposites in the presence of the target analyte DENV ssDNA of all four serotypes in the concentration range of  $10^{-15}$  to  $10^{-9}$  M. (E) Calibration curves for all four DENV serotypes.

terms of the corresponding calibration lines in Fig. 6. The fluorescence spectra of the four target analytes are presented in Fig. 6(A–D), which representing the four serotypes of DENV ssDNAs in the concentration range of  $10^{-15}$  to  $10^{-9}$  M with their individually designed CdSeTeS QD–dsDNA–AuNP nanoprobe. A steady increase in the fluorescence intensity was achieved in the case of DENVs 1 and 3 (Fig. 6(A) and (C)), whereas a decrease in peak intensity was observed in case of DENVs 2 and 4 (Fig. 6(B) and (D)), respectively. The calibration lines from these four graphs are plotted in Fig. 6(E), where linear calibration lines were found for all in the concentration range of  $10^{-15}$  to  $10^{-10}$  M. In the case of  $10^{-9}$  M concentration or higher, the signals tended to saturation. The correlation coefficients were found to be in the range of 0.978 to 0.99. The quenching calibration lines for DENVs 2 and 4 maintained an equal slope; however, the enhanced calibrations for DENVs 1 and 3 changed greatly. Due to the small difference in the content of guanidine bases for all the serotype duplexes, the formation of CdSeTeS QD–dsDNA–AuNP with the analyte ssDNA may be not exactly the same. Since the distance is very sensitive for the LSPR enhancement, the concentration vs. fluorescence signals are slightly varied for each probe, producing different slopes. In addition, the ssDNA probe for DENV 1 forms different types of hairpin structures with a higher energy of  $7 \text{ kcal mol}^{-1}$  compared to that of the other three of  $4.9\text{--}5.1 \text{ kcal mol}^{-1}$ . The most possible secondary structures of all four ssDNA probes are presented in Fig. S4, ESI†. Therefore, due to the more conjugated hairpin, the slope of the enhanced intensity for DENV 1 is lower than that of DENV 3. The limit of detection (LOD) was calculated by  $3 \times$  standard deviation of lowest signal divided by the slope of the calibration line,<sup>45</sup> which was found to be 24.6, 11.4, 39.8 and  $39.7 \text{ fM}$  for DENVs 1, 2, 3 and 4 with the correlation coefficient ( $R^2$ ) of 0.964, 0.963, 0.995 and 0.972, respectively.

#### Detection of four DENV serotypes isolated from real samples with the proposed sensor

After the successful detection of the synthetic small target ssDNAs, the sensing application was extended towards real DENV samples. The aim of the present work is to apply the protocol in direct extracted DENV RNAs without any further pre-treatment or amplification process. Thus, DENV RNAs were extracted from four serotypes of DENV culture fluids and the four types of nanoprobe were used for the analysis. The sequences of the full RNAs are given in Table S1, ESI†. To avoid any secondary loop formation of the RNAs, the RNA samples were incubated at  $95^\circ\text{C}$  for 2 min before the analysis. During the cooling time to normal temperature, the sensor was added to the RNA samples, which helped to make stronger hybridization between the loop region of the nanoprobe with the RNA strand. The stability of the RNAs at  $95^\circ\text{C}$  was also measured by UV-Vis spectroscopy, as presented in Fig. S5, ESI†. As presented in Fig. 7(A), the fluorescence signal of the CdSeTeS QDs was clearly altered depending on the analyte serotype, similar to that of the synthetic ssDNAs in Fig. 5(E). The fluorescence curves are presented in Fig. S6, ESI† for all four samples reacted with all four nanoprobe, and their comparative bar diagram is shown in Fig. 7(A). The percentage changes were not as good as the previous calibration line in DI water. Particularly in the case of DProbe3, the change in fluorescence was 19.2% for DENV 3 with respect to the initial fluorescence, whereas DENV 1, 2 and 4 showed 2.9%, 3.1% and 4.6% respectively. However, considering the presence of interferences in the sample medium, this 4-fold enhancement is acceptable for real analysis, where the concentration of RNA is in the picomolar range. In case of DProbe 1, 2 and 4, the changes were 23.7%,  $-13.4\%$  and  $-12.9\%$ , respectively, for their corresponding targets, where the signals for other interferences were almost negligible. The sensors were then tested for the detection of RNA samples,



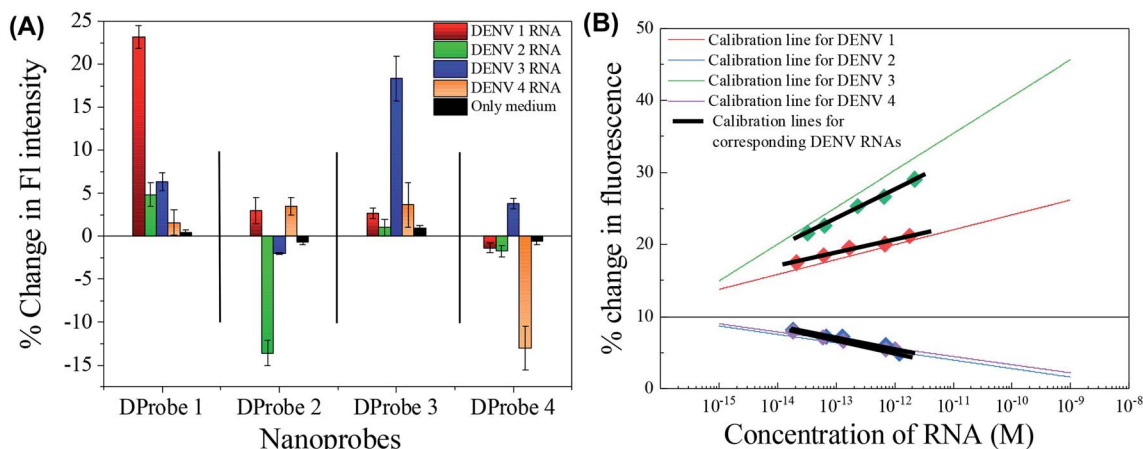


Fig. 7 (A) Comparative analysis of all four nanoprobe in the presence of all four types of DENV RNA serotypes. (B) Quantification of the dengue RNA isolated from DENV culture fluid. Intensities found from the fluorescence of each sample;  $\blacklozenge$  Dengue 1,  $\blacktriangle$  Dengue 2,  $\blacklozenge$  Dengue 3 and  $\blacklozenge$  Dengue 4, quantified from their calibration lines obtained in buffer solution. The black calibration lines are plotted from the RNA concentration.

where the concentration was diluted in four separate solutions to make the proper calibration lines. The percentage changes of the obtained fluorescence for each serotype were plotted in Fig. 7(B) and the corresponding calibration lines were generated. The calibration lines for the real RNA analysis are plotted in bold black lines, which are compared with the calibration lines found in water medium. The 5, 10, 50 and 100-fold diluted results maintained the linearity for all the serotypes. Although the slopes of the calibration lines deviated largely from the water medium, they were still linear. Here, the probe to target binding is DNA/RNA instead of DNA/DNA, which may be the reason for the decrease in the slope. It is obvious that the binding nature of RNA/RNA and RNA/DNA is not exactly the same;<sup>46</sup> however, to understand the trend of binding for the sensing application in this work, the comparison of these two calibration lines is quite satisfactory. All the nanoprobe were also tested with the bare medium, and it was found that the nanoprobe still showed the desired sensitivity for the exact complementary targets even in the complex medium. To confirm the applicability in real sample analysis, evaluation of the different isolates representing the different lineages of each serotype is also required. In future, before proceeding to on-site monitoring, the detectability in the different lineages of each serotype needs to be established. In addition, a few other viral synthetic ssDNAs were also used with the sensor to check any possible non-specific interaction. The Zika virus was chosen since it is from same the flavivirus family of dengue, whereas influenza is a common enveloped virus like dengue. Norovirus was selected as an example of a non-enveloped virus. The nanoprobe showed negligible interactions with the Zika virus and norovirus, as presented in Fig. S7, ESI,<sup>†</sup> confirming the absence of any non-specific interaction from any part of the nanoprobe. In the case of the influenza virus, there was a 1.37-fold enhancement observed compared with the sensor, whereas the target virus of DENV 1 showed a 3.64-fold enhancement, which is quite high to confirm its specific nature. Therefore, from the above results, it can be concluded that the CdSeTeS-ssDNA nanoprobe can successfully identify the DENV

serotypes with the detection of the analyte concentration in DENV culture fluid samples, which can serve as an alternative for point-of-care diagnosis in serotype determination of DENV.

## Conclusions

A sensitive DENV DNA detection biosensor with serotype identification ability was proposed in the present study by altering the distance-based LSPR between AuNPs and CdSeTeS QDs. Four different nanoprobe were constructed using each primer-probe serotype specific hairpin ssDNAs and covalent bonding with CdSeTeS QDs. The synthesized nanoprobe could successfully identify the DENV serotypes, where a fluorescence enhancement was observed for DENVs 1 and 3 and quenching indicated the presence of DENVs 2 and 4. In reaction with free ssDNA-functionalized AuNPs and the nanoprobe, target ssDNA of  $10^{-15}$  to  $10^{-10}$  M was successfully detected. The limit of detection was calculated to be 24.6, 11.4, 39.8 and 39.7 fM for the synthetic ssDNAs of DENVs 1, 2, 3 and 4, respectively. To the best of our knowledge, this is the first attempt for DENV serotype detection together with quantification without any amplification employing the distance-dependent LSPR phenomenon of fluorescent CdSeTeS QDs with adjacent AuNPs. In addition, to confirm its applicability in complex systems, the sensor was also applied to the real DENV RNAs extracted from DENV culture fluids without pre-treatment, which showed satisfactory performances for serotype identification with quantification. This result can make the sensing process a potential diagnostic probe for point-of care detection in the future.

## Conflicts of interest

There are no conflicts to declare.

## Acknowledgements

ADC thanks the Japan Society for the Promotion of Science (JSPS) for a postdoctoral fellowship (No. P17359). This work was



supported and partly by the Bilateral Joint Research Project of the JSPS, Japan.

## References

- 1 L. Zhang, Y. Song, T. Fujita, Y. Zhang, M. Chen and T. H. Wang, *Adv. Mat.*, 2014, **26**, 1289–1294.
- 2 A. L. Feng, M. L. You, L. Tian, S. Singamaneni, M. Liu, Z. Duan, T. J. Lu, F. Xu and M. Lin, *Sci. Rep.*, 2015, **5**, 7779.
- 3 F. Nasrin, A. D. Chowdhury, K. Takemura, J. Lee, O. Adegoke, V. K. Deo, F. Abe, T. Suzuki and E. Y. Park, *Biosens. Bioelectron.*, 2018, **122**, 16–24.
- 4 M. Li, S. K. Cushing, Q. Wang, X. Shi, L. A. Hornak, Z. Hong and N. Wu, *J. Phys. Chem. Lett.*, 2011, **2**, 2125–2129.
- 5 M.-X. Li, W. Zhao, G.-S. Qian, Q.-M. Feng, J.-J. Xu and H.-Y. Chen, *Chem. Commun.*, 2016, **52**, 14230–14233.
- 6 K. Takemura, O. Adegoke, N. Takahashi, T. Kato, T.-C. Li, N. Kitamoto, T. Tanaka, T. Suzuki and E. Y. Park, *Biosens. Bioelectron.*, 2017, **89**, 998–1005.
- 7 Y. Ke, X. Wen, D. Zhao, R. Che, Q. Xiong and Y. Long, *ACS Nano*, 2017, **11**, 7542–7551.
- 8 A. Neely, C. Perry, B. Varisli, A. K. Singh, T. Arbneshi, D. Senapati, J. R. Kalluri and P. C. Ray, *ACS Nano*, 2009, **3**, 2834–2840.
- 9 J. Wang, Y. Shan, W.-W. Zhao, J.-J. Xu and H.-Y. Chen, *Anal. Chem.*, 2011, **83**, 4004–4011.
- 10 C. Li, C. Wu, J. Zheng, J. Lai, C. Zhang and Y. Zhao, *Langmuir*, 2010, **26**, 9130–9135.
- 11 H. Nishi, S. Hiroya and T. Tatsuma, *ACS Nano*, 2015, **9**, 6214–6221.
- 12 X. Zhao, R. Tapeç-Dytioco and W. Tan, *J. Am. Chem. Soc.*, 2003, **125**, 11474–11475.
- 13 A. H. Loo, Z. Sofer, D. Bouša, P. Ulbrich, A. Bonanni and M. Pumera, *ACS Appl. Mater. Interfaces*, 2016, **8**, 1951–1957.
- 14 J.-L. Ma, B.-C. Yin, H.-N. Le and B.-C. Ye, *ACS Appl. Mater. Interfaces*, 2015, **7**, 12856–12863.
- 15 A. D. Chowdhury, R. Gangopadhyay and A. De, *Sens. Actuators, B*, 2014, **190**, 348–356.
- 16 A. Dutta Chowdhury, N. Agnihotri, R.-a. Doong and A. De, *Anal. Chem.*, 2017, **89**, 12244–12251.
- 17 S. Dutta, A. D. Chowdhury, S. Biswas, E. Y. Park, N. Agnihotri, A. De and S. De, *Biochem. Eng. J.*, 2018, **140**, 130–139.
- 18 J. Lee, M. Morita, K. Takemura and E. Y. Park, *Biosens. Bioelectron.*, 2018, **102**, 425–431.
- 19 E. Nebling, T. Grunwald, J. Albers, P. Schäfer and R. Hintsche, *Anal. Chem.*, 2004, **76**, 689–696.
- 20 X. Lu, X. Dong, K. Zhang, X. Han, X. Fang and Y. Zhang, *Analyst*, 2013, **138**, 642–650.
- 21 Y. Zhang, C. Zhu, L. Zhang, C. Tan, J. Yang, B. Chen, L. Wang and H. Zhang, *Small*, 2015, **11**, 1385–1389.
- 22 M. Stanisavljevic, S. Krizkova, M. Vaculovicova, R. Kizek and V. Adam, *Biosens. Bioelectron.*, 2015, **74**, 562–574.
- 23 A. Dutta Chowdhury, A. B. Ganganboina, F. Nasrin, K. Takemura, R.-a. Doong, D. I. S. Utomo, J. Lee, I. M. Khoris and E. Y. Park, *Anal. Chem.*, 2018, **90**, 12464–12474.
- 24 M. N. M. Nuzaihan, U. Hashim, M. M. Arshad, S. Kasjoo, S. Rahman, A. Ruslinda, M. Fathil, R. Adzhri and M. Shahimin, *Biosens. Bioelectron.*, 2016, **83**, 106–114.
- 25 M. A. Iyer, G. Oza, S. Velumani, A. Maldonado, J. Romero, M. d. L. Munoz, M. Sridharan, R. Asomoza and J. Yi, *Sens. Actuators, B*, 2014, **202**, 1338–1348.
- 26 A. A. Odeh, Y. Al-Douri, C. Voon, R. M. Ayub, S. C. Gopinath, R. A. Odeh, M. Ameri and A. Bouhemadou, *Microchim. Acta*, 2017, **184**, 2211–2218.
- 27 N. Mehta, B. Perrais, K. Martin, A. Kumar, T. C. Hobman, M. N. Cabalfin-Chua, M. E. Donald, M. S. S. Painaga, J. Y. Gaite and V. Tran, *Am. J. Trop. Med. Hyg.*, 2019, **100**, 1534–1540.
- 28 E. M. Euliano, A. N. Hardcastle, C. M. Victoriano, W. E. Gabella, F. R. Haselton and N. M. Adams, *Sci. Rep.*, 2019, **9**, 1–11.
- 29 O. Adegoke, T. Nyokong and P. B. Forbes, *J. Alloys Compd.*, 2015, **645**, 443–449.
- 30 S. V. Salihov, Y. A. Ivanenkov, S. P. Krechetov, M. S. Veselov, N. V. Sviridenkova, A. G. Savchenko, N. L. Klyachko, Y. I. Golovin, N. V. Chufarova and E. K. Beloglazkina, *J. Magn. Magn. Mater.*, 2015, **394**, 173–178.
- 31 O. Adegoke, T. Kato and E. Y. Park, *Biosens. Bioelectron.*, 2016, **80**, 483–490.
- 32 O. Adegoke, M. Morita, T. Kato, M. Ito, T. Suzuki and E. Y. Park, *Biosens. Bioelectron.*, 2017, **94**, 513–522.
- 33 O. Adegoke, M.-W. Seo, T. Kato, S. Kawahito and E. Y. Park, *Biosens. Bioelectron.*, 2016, **86**, 135–142.
- 34 M. H. P. Ly, M. L. Moi, T. B. H. Vu, M. M. N. Tun, T. Saunders, C. N. Nguyen, A. K. T. Nguyen, H. M. Nguyen, T. H. Dao and D. Q. Pham, *BMC Infect. Dis.*, 2018, **18**, 31.
- 35 G.-C. Fan, H. Zhu, Q. Shen, L. Han, M. Zhao, J.-R. Zhang and J.-J. Zhu, *Chem. Commun.*, 2015, **51**, 7023–7026.
- 36 C. Zhang, X. Li, C. Tian, G. Yu, Y. Li, W. Jiang and C. Mao, *ACS Nano*, 2014, **8**, 1130–1135.
- 37 S. Krishnamurthy, A. Esterle, N. C. Sharma and S. V. Sahi, *Nanoscale Res. Lett.*, 2014, **9**, 627.
- 38 G.-X. Liang, M.-M. Gu, J.-R. Zhang and J.-J. Zhu, *Nanotechnology*, 2009, **20**, 415103.
- 39 S. M. Watson, H. D. A. Mohamed, B. R. Horrocks and A. Houlton, *Nanoscale*, 2013, **5**, 5349–5359.
- 40 S. R. Ede, A. Ramadoss, S. Anantharaj, U. Nithiyanantham and S. Kundu, *Phys. Chem. Chem. Phys.*, 2014, **16**, 21846–21859.
- 41 A. C. Moço, P. H. Guedes, J. M. Flauzino, H. S. da Silva, J. G. Vieira, A. C. Castro, E. V. Gomes, F. M. Tolentino, M. M. Soares and J. M. Madurro, *Electroanalysis*, 2019, **31**, 1580–1587.
- 42 P. Zhang, T. Beck and W. Tan, *Angew. Chem.*, 2001, **40**, 402–405.
- 43 F. Li, Y. Huang, Q. Yang, Z. Zhong, D. Li, L. Wang, S. Song and C. Fan, *Nanoscale*, 2010, **2**, 1021–1026.
- 44 S. Deng, L. Cheng, J. Lei, Y. Cheng, Y. Huang and H. Ju, *Nanoscale*, 2013, **5**, 5435–5441.
- 45 A. D. Chowdhury, N. Agnihotri, A. De and M. Sarkar, *Sens. Actuators, B*, 2014, **202**, 917–923.
- 46 F. A. Tanious, J. M. Veal, H. Buczak, L. S. Ratmeyer and W. D. Wilson, *Biochemistry*, 1992, **31**, 3103–3112.

